NANO LETTERS

2008
Vol. 8, No. 1
64−68

Unique Carbon-Nanotube Field-Effect Transistors with Asymmetric Source and Drain Contacts

Hong Li,[†] Qing Zhang,*[,†] and Nicola Marzari[‡]

Microelectronics Center, School of Electrical and Electronics Engineering, Nanyang Technological University, S1-B2c-20, Singapore 639798, and Department of Materials Science and Engineering, 13-5066 MIT, 77 Massachusetts Avenue, Cambridge, Massachusetts 02139-4307

Received August 3, 2007; Revised Manuscript Received November 12, 2007

ABSTRACT

We have fabricated a type of unique single-walled carbon nanotube field-effect transistor, in which the channel length is only 90 nm and aluminum and gold are used as its drain and source electrodes, respectively. The channel conductance oscillations caused by single-electron tunneling through the asymmetric barriers at the drain and source contacts are observed up to 100 K. Above 100 K, the tunneling fades away, and thermionic emission dominates the conductance at sufficiently negative gate voltages. At room temperature, the device shows diode-like characteristics with a maximum current rectification ratio of ~10^4.

Single-walled carbon nanotubes (SWNTs) are of great interest from fundamental physics and nanoelectronic application points of view because of their unique electronic properties and quasi-one-dimensionality.[1,2] Since the first demonstration of carbon nanotube (CNT) field-effect transistors (FETs) by Tans et al. and Martel et al. in 1998,[3] a variety of interesting CNT-based devices have been developed with FET geometry, including CNT-based chemical and biological sensors,[4,5] nonvolatile memory cells,[6,7] diodes,[8−10] single electron/hole transistors (SETs/SHTs),[11−14] and so forth. Among them, CNT-based SETs/SHTs have attracted a lot of attention. Single-electron charging in a short SWNT bundle (~200 nm in length) was first reported by Bockrath et al. in 1997.[12] Later on, Postma et al. demonstrated a room-temperature SET using a metallic SWNT with a short kink (~25 nm) created by mechanically bending the SWNT using an atomic force microscope (AFM).[13] Cui et al. reported a room-temperature SET by local chemical modification (~10 nm in length) of a SWNT bundle.[14] However, almost all reported studies have focused on SETs/SHTs with similar capacitive couplings to the drain (D) and source (S) electrodes, i.e., symmetric D−S contacts.

In this paper, we report on a type of short-SWNT-channel FET with asymmetric D and S electrodes (channel length ~ 90 nm). The asymmetric barriers result in unequal conductance oscillations at low temperatures. Moreover, the devices exhibit remarkable current rectification characteristics at room temperature.

Raman spectrum and transmission electron microscopy images show that SWNTs used in this work have uniform diameter ($D \approx 1.4$ nm), from which the band gap of the semiconducting one can be estimated as $E_g \approx 0.9/D \approx 0.6$ eV.[1] A self-alignment technique (shadow electron-beam evaporation) was employed to define a very short SWNT channel.[15] A schematic structure and an AFM image of a device with a channel length of ~90 nm are shown in Figure 1a,b, respectively. The left portion of the SWNT-channel is sandwiched between SiO_2 and an Al pad (low work function, $\Phi_{Al} \approx 4.3$ eV),[16] and hence the electrical properties of the contact are determined by Al/SWNT coupling. In contrast, the right portion of the SWNT attaches to the sidewall of a Au electrode (high work function, $\Phi_{Au} \approx 5.2$ eV) so that the contact properties depend on Au/SWNT coupling. The results reported here were obtained using the Al electrode as the drain and the Au electrode as the source. The height of the SWNT channel is 5 nm from the AFM measurements. The back-gate dielectric is 0.5-μm-thick thermally grown SiO_2.

At 25 K, strong oscillations in the SWNT-channel current (I_{DS}) as a function of gate voltages (V_{GS}) are observed, as shown in Figure 2a. The temperature-dependent transfer curves at $V_{DS} = +30$ mV are shown in the inset. The linear scale plots of the oscillations with both positive and negative V_{DS} are presented in Figure 2b, where the curves at equal $|V_{DS}|$ are plotted with the same color. Owing to a large I_{on}/

* Corresponding author. Tel.: +65 67905061. Fax: +65 67920415. E-mail address: eqzhang@ntu.edu.sg.
[†] Nanyang Technological University.
[‡] MIT.

10.1021/nl071905e CCC: $40.75
Published on Web 12/11/2007

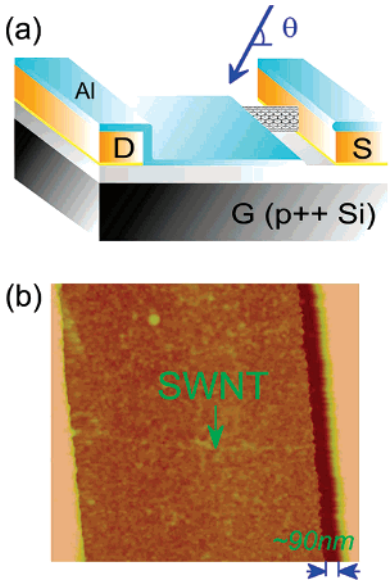

Figure 1. Short-SWNT-channel FET. (a) A schematic diagram of the device structure. (b) An AFM image of an ~90-nm-channel CNTFET. The arrow indicates the SWNT.

I_{off} ratio (~10^7), some oscillation peaks could not be reflected in this linear plot, where only the peaks near $V_{GS} \sim -10$ V are clearly presented. Figure 2c shows the contour plot of $\log|I_{DS}|$ in the $V_{DS}-V_{GS}$ plane. Three "diamond"-shaped current suppression regions are seen. These observations could be interpreted by the Coulomb blockade effect[17] in an SET[12,18] (see the inset of Figure 2b for the equivalent circuit), in which the barriers at the two metal/SWNT contacts[19] serve as tunneling capacitors (C_1 and C_2). Due to its small volume, the short SWNT-channel could be viewed as an "island" with discrete energy levels (E_i). Whenever the Fermi levels of the S and D electrodes line up with one of E_i, a conductance peak due to single-electron tunneling occurs. With increasing temperature, the thermal energy (k_BT) becomes comparable to or even larger than the Coulomb charging energy (e^2/C_Σ, where $e = -1.6 \times 10^{-19}$ C is the electron charge, and C_Σ is the total capacitance to the SWNT "island").[12] As a result, the oscillation peaks broaden and fade away when T is above 100 K, as shown in the inset of Figure 2a.

The observed Coulomb oscillations possess two notable characteristics. First of all, the peak-to-valley ratio can be as high as 1 order of magnitude, and the peaks are situated at different I_{DS} levels. In other words, I_{DS} could be viewed as the Coulomb oscillations superimposed upon a transfer curve of a CNTFET. Thus, the roles of V_{GS} are twofold here: (1) to manipulate the positions of discrete energy levels, E_i, and (2) to control the carrier density in the SWNT channel (through the SWNT−bulk and/or contact barrier modulation).[19,20] Second, the amplitude of the current under negative V_{DS} are larger than the corresponding one under positive V_{DS}, as shown in Figure 2b, where the dashed line indicates $V_{DS} = 0$. As a result, the "diamond"-shaped regions confined by a pair of oscillation peaks (with equal $|V_{DS}|$) shift downward as delineated by the dashed arrow. We attribute the asymmetric current oscillations to the difference between the Al/SWNT and Au/SWNT contacts ($C_1 > C_2$).

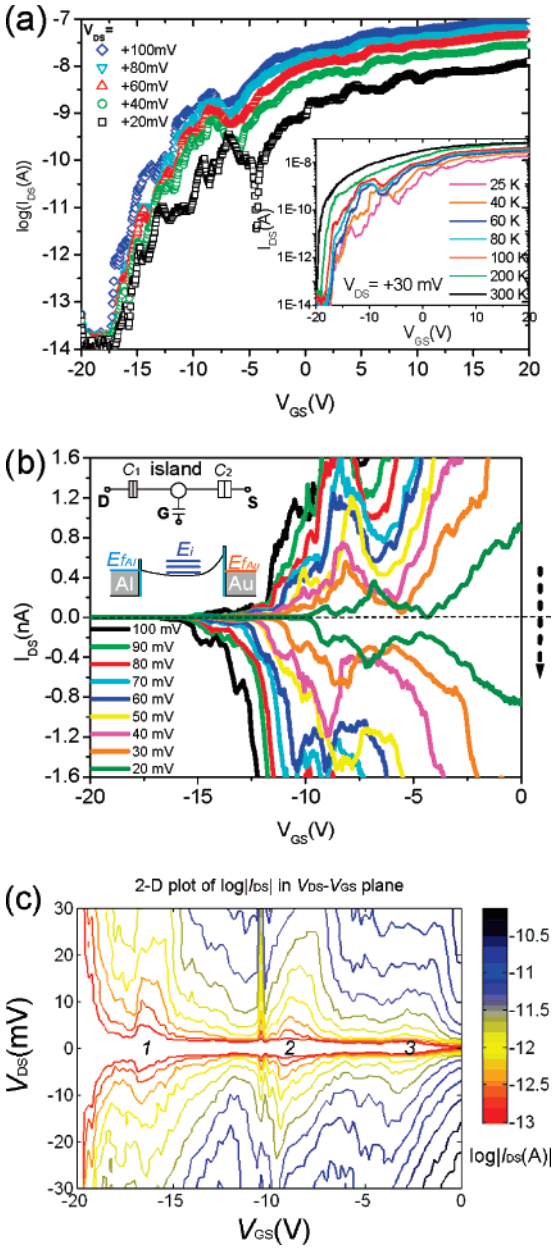

Figure 2. Low-temperature n-type characteristics of the SWNT FET. (a) $I_{DS}-V_{GS}$ curves (logarithmic scale) at $T = 25$ K with V_{DS} ranging from +20 to +100 mV in steps of 20 mV. Inset: $I_{DS}-V_{GS}$ curves (logarithmic scale) at $V_{DS} = +30$ mV and temperatures ranging from 25 up to 300 K. (b) $I_{DS}-V_{GS}$ curves (linear scale) at $T = 25$ K for $V_{GS} = -20$ to 0 V with V_{DS} ranging from −100 to +100 mV in steps of 20 mV (I_{DS} with equal $|V_{DS}|$ are plotted in the same color.). Inset: a schematic conduction band alignment and equivalent SET circuit. Extra barriers besides SB are inserted between metals and SWNT. (c) The contour plot of $\log|I_{DS}|$ in the $V_{DS}-V_{GS}$ plane. $\log|I_{DS}|$ is color-coded, as shown by the color bar. The innermost contour line represents $|I_{DS}| \sim 100$ fA.

Evidence of the asymmetric contacts can be obtained from the Coulomb "diamonds" shown in Figure 2c. Assuming that a single electron is involved in each tunneling event,[21] we can give a quantitative description using the SET circuit. As the average gate modulation period of the three Coulomb "diamonds" is $\Delta V_{GS} \approx 7$ V, the gate capacitance should be $C_{GS} = (|e|)/(\Delta V_{GS}) \approx 0.02$ aF. From the slopes of the boundaries of the Coulomb "diamonds", the coupling

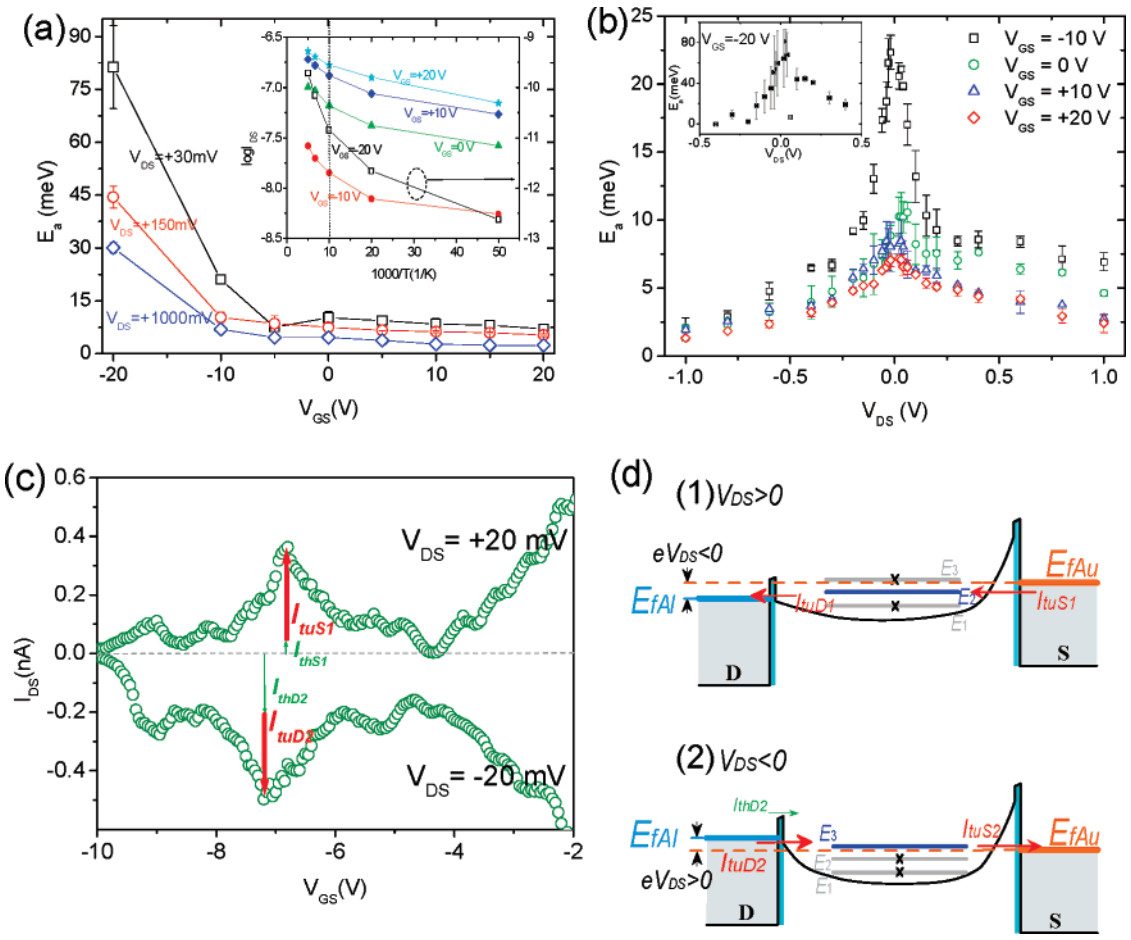

Figure 3. (a) E_a versus V_{GS} at $V_{DS} = +30$, $+150$, and $+1000$ mV, respectively. Error bars are introduced as a result of the linear fit of the Arrhenius plot for E_a estimation. Inset: log I_{DS} versus $1000/T$ plot at $V_{DS} = +150$ mV for $V_{GS} = -20$, -10, 0, $+10$, and $+20$ V, respectively. (b) E_a versus V_{DS} at $V_{GS} = -10$, 0, $+10$, and $+20$ V (from top to bottom), respectively. Inset: E_a versus V_{DS} at $V_{GS} = -20$ V (The large error bars are caused by the poor signal-to-noise ratio since the device is in the "OFF" state with $V_{GS} = -20$ V). (c) $I_{DS}-V_{GS}$ curves at $V_{DS} = \pm 20$ mV with V_{GS} ranging from -10 to -2 V (the innermost curves in Figure 2b). I_{tuS1} and I_{tuD2} mark the oscillation height (single-electron tunneling current) for positive and negative V_{DS}, respectively, and I_{thS1} and I_{thD2} label the background current (thermionic emission current) for positive and negative V_{DS}, respectively. (d) Schematic energy band diagrams for (1) positive and (2) negative V_{DS}. I_{th} and I_{tu} indicate thermionic emission and single-electron tunneling current components, respectively. Blue color represents E_i involved in single-electron tunneling, and gray color delineates E_i that are not involved in electron transport. The cyan regions represent the extra barriers besides SB.

capacitances at Al/SWNT and Au/SWNT contacts can be estimated as $C_1 \approx 2.5$ aF and $C_2 \approx 1.3$ aF, respectively.[22] This indicates that the coupling at the Al/SWNT contact is stronger than that at the Au/SWNT contact. The total capacitance is $C_\Sigma = C_{GS} + C_1 + C_2 \approx 3.8$ aF. Comparing this with another simple estimation, $C_\Sigma \approx \epsilon_0\epsilon_r l$,[23] where l is the length of SWNT "island" and $\epsilon_r \approx 4$ for SiO_2, we obtain $l \sim 110$ nm, and this value is reasonably consistent with the 90 nm measured by an AFM. Such a small C_Σ causes a charging energy of $E_C = e^2/C_\Sigma \approx 42$ meV, which is much larger than k_BT ($T < 100$ K), indicating satisfaction of the necessary condition for observing single-electron tunneling. The conversion factor from the gate voltage to the electrostatic potential of the SWNT-channel is $E_C/|e\Delta V_{GS}| \approx 0.006$. The small conversion factor could be attributed to the short SWNT-channel length and relatively thick back-gate oxide (0.5 μm). The discrete energy level spacing for electrons confined to a one-dimensional box is estimated as $\Delta E = (dE/dk)(\Delta k/2) = \hbar v_F(\pi/2l) \approx 0.8/l$ (meV), where l is the length of the box in μm, $v_F \approx 8 \times 10^5$ m/s is the Fermi velocity of graphite, and the factor of 1/2 accounts for the nondegeneracy of the two one-dimensional subbands. $\Delta E \approx 9$ meV is obtained with $l = 90$ nm, and it is comparable to k_BT for $25 < T < 100$ K. Therefore, one or more discrete energy levels may be involved in a tunneling event.

Another evidence of the asymmetric contacts comes from the contact barrier heights. As pointed out by Appenzeller et al.,[24] the channel conductance of CNTFETs depends on both tunneling and thermionic emission. The barrier height (activation energy E_a) can be estimated from the thermionic emission current (in the temperature range above 100 K, as shown in the inset of Figure 3a).[24] From the E_a-V_{GS} plot shown in Figure 3a, one can see that E_a increases drastically from 20 to 80 meV for $V_{DS} = +30$ mV when $V_{GS} < -10$ V, implying that the tunneling current is fading away. In other words, the majority of electrons are thermionically injected into the SWNT channel when $V_{GS} < -10$ V, while tunneling is a dominant process when $V_{GS} > -10$ V. It is noted that

the extracted activation energies are very small. Chen et al. also reported small E_a and attributed their observations to the p-type chemical doping due to air.[25] However, their explanations do not account for our case, since our device shows strong n-type characteristics. We suggest that the small E_a is caused by imperfect contacts since the devices were fabricated using ac dielectrophoresis technique, and a thin layer of Triton X 100 between SWNT and metals could be introduced. In addition to the Schottky barrier (SB), an extra tunneling barrier (cyan regions in the inset of Figure 2b) could be formed at the metal/SWNT interfaces. As a result, some of the electrons have to tunnel through the extra barrier before being thermionically emitted over the SB. Thus, E_a becomes an effective barrier height, which could be smaller than the barrier height estimated from pure thermionic emission over a SB. Interestingly, one can see that the values of E_a at positive V_{DS} (right branches) are larger than those at the corresponding negative V_{DS} (left branches) by a factor of >2 for all V_{GS} (see Figure 3b). Since the Al and Au pads are connected as the D and S electrodes, respectively, electrons feel the SB at the Al/SWNT (Au/SWNT) contact when V_{DS} is negative (positive). Thus, the SB height is expected to be larger when V_{DS} is positive because the Fermi level of Au is closer to the valence band of SWNTs ($\Phi_{SWNT} \sim 4.8$ eV) in comparison with Al. However, the work functions used for Al and Au are for the materials in vacuum, and they can be affected by the adsorbed molecules. As a result, the observed SB height should be influenced in different chemical environments.

The transfer curves for $V_{DS} = \pm 20$ mV are selected from Figure 2b and replotted in Figure 3c. I_{DS} consists of two components: (1) oscillation current probably caused by a single-electron tunneling process, I_{tuS1} and I_{tuD2}, and (2) background current likely resulting from thermionic emission, I_{thS1} and I_{thD2}, as indicated in Figure 3c. The subscripts "tu" and "th" stand for tunneling and thermionic emission, respectively, "1" and "2" represent positive (Case 1) and negative (Case 2) V_{DS} bias, respectively, and "S" and "D" mean the source and drain, respectively. The electron transport mechanisms are illustrated in Figure 3d. For simplicity, the discrete energy levels E_i are assumed to be stationary with respective to the Fermi level of the Au electrode E_{fAu} (common) when V_{GS} is fixed. For a positive V_{DS} (Case 1), the energy level E_2 is situated between E_{fAl} and E_{fAu} so that electrons from the S side (I_{tuS1}) could tunnel through E_2 to the D barrier (I_{tuD1}), as shown in Figure 3d (1). I_{thS1} in Figure 3c is negligible, thus, $I_{DS} \sim I_{tuS1}$ could be obtained. In contrast, when V_{DS} is negatively biased (Case 2), the energy level E_3 is situated between E_{fAl} and E_{fAu}, so that electrons could tunnel through the D barrier (I_{tuD2}) and then E_3 to the S barrier (I_{tuS2}). Moreover, since the barrier at the Al/SWNT contact is small, some electrons could be thermionically injected over the barrier (I_{thD2}). Thus, $I_{DS} \sim I_{tuD2} + I_{thD2}$ is obtained in this case. As shown in Figure 3c, $I_{tuS1} \sim I_{tuD2}$, i.e., the single-electron tunneling currents in both cases are comparable. This observation indicates that electron tunneling rates are not significantly influenced by changing the polarity of V_{DS}. In contrast, $I_{thD2} \gg I_{thS1}$ is seen in Figure 3c, i.e., the thermionic emission current for a negative V_{DS} is much more significant than that for a positive V_{DS}. In other words, the unequal current amplitude is mainly caused by difference between the thermionic emission current over the uneven contact barriers, instead of single-electron tunneling current.

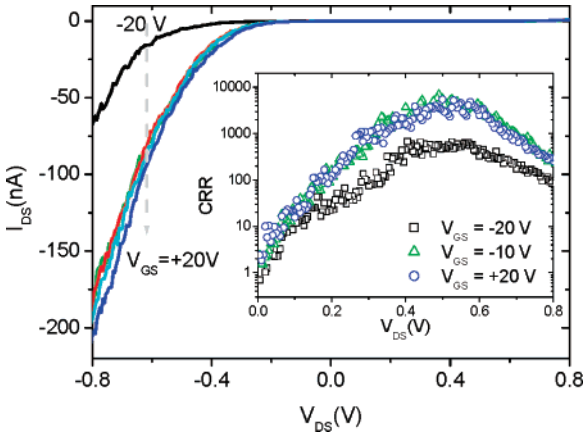

Figure 4. The diode-like characteristics at room temperature. $I_{DS}-V_{DS}$ curves at different V_{GS} (from -20 to $+20$ V in step of 10 V) at room temperature in air. Inset: CRRs at $V_{GS} = -20$, -10, and $+20$ V, respectively.

At room temperature in air, striking current rectification characteristics[26,27] are observed and shown in Figure 4. The current rectification ratios (CRRs), defined as the relative change in I_{DS} when V_{DS} is reversed,[28] i.e., $I_{DS}(-|V_{DS}|)/I_{DS}(|V_{DS}|)$, are shown in the inset. As discussed above, I_{DS} is dominated by thermionic emission at $V_{GS} < -10$ V and $T > 100$ K. From the thermionic emission model, CRR $= I_{DSFB}/I_{DSRB} \approx \exp[(e(E_{aFB} - E_{aRB}))/(k_BT)]$, where the subscripts "FB" and "RB" stand for forward and reverse D−S bias, respectively. At 300 K and $V_{GS} = -10$ V, a maximum CRR is ≈ 7000 at $V_{DS} \approx 0.5$ V (see green triangles in the inset of Figure 4), and hence, the barrier height difference, $E_{aFB} - E_{aRB} \approx [(k_BT)/e] \ln(I_{DS_{FB}}/I_{DS_{RB}}) \approx -0.23$ eV. However, this difference could be caused not only by SB differences, but also by imperfect contacts, environmental influences,[25] dipole effects,[29] and so forth.

The n-type conduction in our devices could be attributed to the stronger coupling of Al/SWNT compared to that of Au/SWNT. The barrier at a metal/SWNT contact depends on the work functions of the two materials and the metal/SWNT interfacial structures. Shan et al. showed that the Fermi level alignment at the metal/nanotube contact could depend on the interfacial distance.[30] More recently, Moon et al. experimentally and theoretically observed n-type CNTFETs with large-work-function metal electrodes, such as Co and Au. They attributed the conduction type of CNTFETs to the microscopic differences of the contacts.[31] In our case, one end of the SWNT is covered by an Al electrode, while the other end is attached to the sidewall of a Au electrode. Thus, it is likely to have a stronger Al/SWNT coupling than Au/SWNT coupling. Moreover, our previous work showed that Triton X 100 (as surfactant) could change CNTFETs with Au electrodes from p-type to ambipolar, suggesting that the SB for holes at Au/SWNT is increased

by Triton X 100.[32] Therefore, the effects of stronger Al/SWNT coupling and influences of Triton X 100 could result in lower effective barriers to the conduction band, leading to n-type conduction.

In conclusion, short-SWNT-channel FETs with asymmetric source and drain electrodes are fabricated. Coulomb oscillation peaks superimposed on the transfer curves of the n-type FETs are observed up to 100 K. The oscillation current amplitudes are found to be asymmetric under positive and negative V_{DS}, and the asymmetric current amplitude is mainly caused by an unequal thermionic emission current over the different barrier heights at the drain/source contacts. The barrier height at the Au/SWNT contact is larger than that at the Al/SWNT contact by a factor of >2 for all V_{GS}. In an atmosphere environment, the device shows significant diode-like effects with a maximum CRR of $\sim 10^4$.

Acknowledgment. We acknowledge generous support of this work by MOE AcRF Tier 2 Funding (ARC17/07, T207B1203) and the Singapore−MIT Alliance.

Supporting Information Available: Details of the experimental methods. This material is available free of charge via the Internet at http://pubs.acs.org.

References

(1) Avouris, Ph.; Appenzeller, J.; Martel, R.; Wind, S. J. *Proc. IEEE* **2003**, *91*, 1772.
(2) Avouris, Ph. *Acc. Chem. Res*. **2002**, *35*, 1026.
(3) Tans, S. J.; Verschueren, A. R. M.; Dekker, C. *Nature* **1998**, *393*, 49. Martel, R.; Schmidt, T.; Shea, H. R.; Hertel, T.; Avouris, Ph. *Appl. Phys. Lett.* **1998**, *73*, 2447.
(4) Kong, J.; Franklin, N. R.; Zhou, C.; Chapline, M. G.; Peng, S.; Cho, K.; Dai, H. *Science* **2000**, *287*, 622.
(5) Liu, N.; Cai, X.; Lei, Y.; Zhang, Q.; Chan-Park, M. B.; Li, C.; Chen, W.; Mulchandani, A. *Electroanalysis* **2007**, *19*, 616.
(6) Fuhrer, M. S.; Kim, B. M.; Dürkop, T.; Brintlinger, T. *Nano Lett.* **2002**, *2*, 755.
(7) Yang, D. J.; Zhang, Q.; Wang, S. G.; Zhong, G. F. *Diamond Relat. Mater*. **2004**, *13*, 1967.
(8) Zhou, C.; Kong, J.; Yenilmez, E.; Dai, H. *Science* **2000**, *290*, 1552.
(9) Fuhrer, M. S.; Nygård, J.; Shih, L.; Forero, M.; Yoon, Y-G.; Mazzoni, M. S. C.; Choi, H. J.; Ihm, J.; Louie, S. G.; Zettl, A.; McEuen, P. L. *Science* **2000**, *288*, 494.
(10) Freitag, M.; Radosavljević, M.; Zhou, Y.; Johnson, A. T.; Smith, W. F. *Appl. Phys. Lett.* **2001**, *79*, 3326.
(11) Li, H.; Zhang, Q.; Li, J. *Appl. Phys. Lett.* **2006**, *88*, 013508.
(12) Bockrath, M.; Cobden, D. H.; McEuen, P. L.; Chopra, N. G.; Zettl, A.; Thess, A.; Smalley, R. E. *Science* **1997**, *275*, 1922.
(13) Postma, H. W. Ch.; Teepen, T.; Yao, Z.; Grifoni, M.; Dekker, C. *Science* **2001**, *293*, 76.
(14) Cui, J. B.; Burghard, M.; Kern, K. *Nano Lett.* **2002**, *2*, 117.
(15) Javey, A.; Qi, P.; Wang, Q.; Dai, H. *Proc. Natl. Acad. Sci. U.S.A.* **2004**, *101*, 13408.
(16) Lu, C.; An, L.; Fu, Q.; Liu, J.; Zhang, H.; Murduck, J. *Appl. Phys. Lett.* **2006**, *88*, 133501.
(17) Mehrez, H.; Guo, H.; Wang, J.; Roland, C. *Phys. Rev. B* **2001**, *63*, 245410.
(18) Takahashi, Y.; Ono, Y.; Fujiwara, A.; Inokawa, H. *J. Phys.: Condens. Matter* **2002**, *14*, R995.
(19) Heinze, S.; Tersoff, J.; Martel, R.; Derycke, V.; Appenzeller, J.; Avouris, Ph. *Phys. Rev. Lett.* **2002**, *89*, 106801.
(20) Javey, A.; Guo, J.; Farmer, D. B.; Wang, Q.; Wang, D.; Gordon, R. G.; Lundstrom, M.; Dai, H. *Nano Lett.* **2004**, *4*, 447.
(21) For simplicity, we assume that a single electron is involved in an individual tunneling event so that we could estimate the relevant electrical parameters using a simple model. Actually, more than one electron (energy states) may be involved in an individual tunneling event. However, our concern here is to see different contact couplings between the Al/SWNT and Au/SWNT.
(22) Roschier, L.; Penttilä, J.; Martin, M.; Hakonen, P.; Paalanen, M.; Tapper, U.; Kauppinen, E. I.; Journet, C.; Bernier, P. *Appl. Phys. Lett.* **1999**, *75*, 728.
(23) Nygård, J.; Cobden, D. H.; Bockrath, M.; McEuen, P. L.; Lindelof, P. E. *Appl. Phys. A* **1999**, *69*, 297.
(24) Appenzeller, J.; Radosavljević, M.; Knoch, J.; Avouris, Ph. *Phys. Rev. Lett.* **2004**, *92*, 048301.
(25) Chen, Y.-F.; Fuhrer, M. S. *Nano Lett.* **2006**, *6*, 2158.
(26) Kim, B.-K.; Kim, J.-J.; So, H.-M.; Kong, K.; Chang, H.; Lee, J.-O.; Park, N. *Appl. Phys. Lett.* **2006**, *89*, 243115.
(27) Yang, M. H.; Teo, K. B. K.; Milne, W. I.; Hasko, D. G. *Appl. Phys. Lett.* **2005**, *87*, 253116.
(28) Iovan, A.; Haviland, D. B.; Korenivski, V. *Appl. Phys. Lett.* **2006**, *88*, 163503.
(29) Yamada, T. *Phys. Rev. B* **2004**, *69*, 125408.
(30) Shan, B.; Cho, K. *Phys. Rev. B* **2004**, *70*, 233405.
(31) Moon, S.; Lee, S-G.; Song, W.; Lee, J. S.; Kim, N.; Kim, J.; Park, N. *Appl Phys. Lett.* **2007**, *90*, 092113.
(32) Li, J.; Zhang, Q.; Li, H.; Chan-Park, M. B. *Nanotechnology* **2006**, *17*, 668.

NL071905E